BULLETIN OF THE POLISH ACADEMY OF SCIENCES
TECHNICAL SCIENCES, Vol. 73(5), 2025, Article number: e154724
DOI: 10.24425/bpasts.2025.154724

Investigation of the ability to manipulate light polarization properties in a liquid crystal cell filled with ferronematic material through electric and magnetic fields

Joanna KOREC-KOSTUREK[1]*, Michał NIEWCZAS[2], Jerzy DZIADUSZEK[1], Przemysław KULA[1], Rafał ZBONIKOWSKI[3], Jan PACZESNY[3] and Karol A. STASIEWICZ[1]

[1] Faculty of Advanced Technologies and Chemistry, Military University of Technology, Kaliskiego 2, 00-908 Warsaw, Poland
[2] Institute of Micromechanics and Photonics, Warsaw University of Technology, A. Boboli 8, 02-525 Warsaw, Poland
[3] Polish Academy of Sciences, M. Kasprzaka 44/52, 01-224 Warsaw, Poland

Abstract. This research paper investigates the integration of liquid crystals doped with magnetic nanoparticles into optical fiber systems to examine changes in light propagation parameters, with emphasis on polarization. The study leverages the unique anisotropic properties of LCs and the tunable characteristics introduced by MNPs for novel sensor applications. Various concentrations of MNPs (from 0.1 to 0.5 wt%) are introduced into the 6CHBT liquid crystal matrix, and the effects of electric and magnetic fields on polarization parameters such as azimuth and ellipticity are analyzed. Results show significant exponential changes in these parameters occurring at a doping concentration of 0.1 wt% and stabilizing above 120 V, while higher concentrations yield smaller linear changes. The polarization direction shifts from left- to right-handed with increasing concentrations of MNPs, and applying a magnetic field intensifies these effects. Overall, this paper demonstrates the potential of the developed system for applications such as tunable optical filters and sensors for temperature, magnetic, and electric fields.

Keywords: magnetic nanoparticle; Fe_3O_4 NPs; liquid crystal; ferronematic; polarization measurement; in-line sensor.

1. INTRODUCTION

One of the fastest-developing fields in technology and materials science today is liquid crystals (LC). Some of the most important areas of life where LCs are used include displays [1], temperature sensors [2–4], solar cells [5,6], biomedical applications [7,8], light propagation systems [9–11], and many others. As widely described in the literature [12, 13], LCs possess a unique structure of elongated molecules that facilitates the introduction of anisotropic properties of refractive indices, referred to as ordinary n_o and extraordinary n_e. These properties are present at temperatures below the isotropic point, above which anisotropy disappears. Not only does temperature affect the refractive indices, but applying the appropriate voltage can cause the reorientation of molecules, which in turn corresponds to changes in the refractive index.

Another rapidly developing field is optical fiber technology. Nowadays, much research is focused on data transmission and using standard and photonic optical fibers to create a new highly sensitive sensor. Some of the most exciting applications of this technology are in medicine [14, 15], energy conversion [16], environmental monitoring [17, 18], aerospace [18], food safety [19, 20], and plasmon resonance sensors [21, 22]. The essential advantages of optical fiber sensors include immunity to electromagnetic interference, low weight, small size, high sensitivity, large bandwidth, and ease of optical signal transmission.

While each of the aforementioned technologies presents unique strengths, they also exhibit inherent limitations, as outlined earlier. A new approach that could lead to the development of novel types of sensors or help discover new phenomena is a hybrid technology combining these two fields. An analysis of the literature shows that such solutions are becoming increasingly popular and are being explored by many research groups using various methods to combine liquid crystals and optical fibers. Among the most extensively studied combinations of these two technologies is filling the air holes in a photonic crystal fiber (PCF) [23–25], which allows for changes in the effective refractive index, with LC used as additional material in a polished standard single-mode fiber (SMF) region [26] or as cladding in a tapered optical fiber (TOF) [27,28] to increase sensitivity or to enhance the interaction between the leaked beam and the added material.

An increasing amount of research focuses on the possibility of controlling light beam parameters with external factors such as temperature, humidity, pressure, electric fields, magnetic fields, and others. Many materials are sensitive only to specific factors, like LC for temperature and electric fields [25]. Combinations of

*e-mail: joanna.korec@wat.edu.pl

Manuscript submitted 2024-11-13, revised 2025-03-20, initially accepted for publication 2025-05-17, published in August 2025.

different types of materials are often used to extend the influence of other factors on a base element. Currently, nanomaterials are undergoing rapid development and are being incorporated in various areas such as drug delivery [29], chemical and biological sensing [30], gas sensing [31, 32], CO_2 capture [33], and other related applications [34]. Nanoparticles can also be used as additional materials to influence or modify the properties of base materials, including optical properties.

Researchers pay special attention to magnetic nanoparticles when analyzing the properties of both fiber optic and liquid crystal technologies. The possibility of using a magnetic field to change or control the parameters of a light beam in optical fiber elements was the main goal assumed by the authors. Recently, many studies have reported on filling the air holes of PCF with magnetic fluid [12], pure LCs [23], or surrounding tapers with magnetic fluid [35], as a detector of different acids [36], magnetometer [37] or magnetic field sensors [38]. This research continues the authors' latest article [39] and focuses on doping LCs with magnetic nanoparticles and measuring changes in light propagation parameters, including polarization.

The following section of the paper outlines the key materials, such as fibers, liquid crystals, magnetic nanoparticles, and setups for measuring polarization parameters, all of which are essential for obtaining the anticipated results.

2. MATERIALS AND METHODS

2.1. Materials for LC devices

The basic element in which the optical beam is controlled or modified is the SMF-28 single-mode fiber from Corning (Corning, NY, USA). The choice of this fiber optic cable was dictated primarily by its ubiquity in applications, low cost, and single-mode operation in the telecommunications range, for which most measurement and transmission equipment is currently calibrated worldwide. The most important parameters include a cut-off wavelength of 1220–1300 nm, mode field diameter of 8.8–9.6 μm @1310 nm and 9.9–10.9 μm @1550 nm, core diameter of 8.2 μm, and maximum attenuation of 0.32/0.18 dB/km @1310/1550 nm [40]. To influence the beam propagated inside the fiber, it is necessary to change the boundary conditions, especially enabling interaction with the evanescent field [41, 42] of the propagating light. The solution proposed in this paper and our previous reports is based on a tapering process. This process reduces the optical fiber diameter and simultaneously increases the penetration depth of the evanescent wave, facilitating interaction with additional materials such as LCs, metals, alkanes, and others. A structure that incorporates a taper and additional materials is referred to as a double-clad structure [43].

In our investigation, we used a taper manufacturing system called fiber optic taper element technology (FOTET), employing a low-pressure gas burner torch. Previous articles have extensively described the setup and detailed operating principles [10, 36, 40]. This approach allows for manufacturing tapers with a waist diameter $\varphi = 14.50 \pm 0.50$ μm and insertion loss below $\alpha = 0.2$ dB @1550 nm (adiabatic taper profile), using different types of fibers. The length of such tapers was approximately $L = 20.20 \pm 0.05$ mm, which facilitated the optimization of the LC device in terms of both LC usage and the external dimensions of the cells. The thickness of the LC cell containing the taper was optimized with respect to the voltages necessary for full LC-molecule reorientation and the spacer thickness of 40 μm [39].

The research used an optical fiber taper enclosed in liquid crystal cells filled with a ferronematic. A ferronematic is a stable colloidal suspension of monodomain ferromagnetic particles in a nematic LC host. Introducing nanoparticles allows for improving the electro- or magneto-optical properties of liquid crystals via a nonchemical method. When a magnetic field is applied, the magnetic particles change the orientation and direction of the LC molecules due to the coupling between the nanoparticles and the LC molecules [39].

This study used the thermotropic nematic 6CHBT (4-trans-4-n-hexylcyclohexyl-isothiocyanatobenzene), a low-melting LC with high chemical stability [44], provided by the Military University of Technology. All parameters were introduced in our previous research. The LC samples were doped with a magnetic suspension consisting of Fe_3O_4 particles with an average diameter of 10 nm. To avoid aggregation of the magnetic nanoparticles (MNPs), they were coated with oleic acid as a surfactant. The doping process was performed by simply adding the suspension under continuous stirring. Measurements were conducted for mixtures with different weight concentrations of magnetic particles: 0.1%, 0.2%, and 0.5%. When particles are placed in a nematic LC, they cause deformations and topological defects in the LC. A key characteristic of LC colloidal dispersions is that elastic distortions of the director and disruption of the local order parameter near the MNPs lead to LC-mediated interactions between the particles. These interactions are not present in typical colloidal dispersions with isotropic fluids. As a result, MNPs show a much stronger tendency to aggregate in the anisotropic LC phase compared to the isotropic phase. The nematic mesophase develops when the temperature drops below the clearing point, leading to spontaneous MNP aggregation.

The measurement setup for broad-spectrum measurements included a SuperK EXTREME supercontinuum light source from NKT Photonics, coupled to the LC cell with ferronematic, while spectral analysis was performed using a Yokogawa AQ6375 optical spectrum analyzer (OSA). The electric field, which controlled the alignment of LC molecules inside the cell, was generated using a Rigol DG4062 signal generator connected to an FLC A400D voltage amplifier. The magnetic field was induced by a pair of N42 neodymium magnets ($10 \times 10 \times 10$ mm) with remanence induction Br: 1.28–1.32 T, coercivity HcB: min. 923 kA/m, coercivity HcJ: min. 955 kA/m, and maximum magnetic energy density (BH)max: 318–342 kJ/m^3, placed on both sides of the LC cell.

The polarization measurement system consisted of a TSL-210 tunable laser from Santec, connected to a manual fiber polarization controller. The polarization state was analyzed using a PAX polarimeter with an external sensor head PAN5710IR3 (Thorlabs). This polarimeter has a high dynamic range of 70 dB and provides azimuth and ellipticity accuracies of ±0.25° on the Poincaré sphere, as shown in Fig. 1. The LC cell electric con-

trol system was the same as in the first measurement setup. All proposed measurements were conducted at room temperature on a passive, vibration-isolated optical table. All measurements were repeated at least five times.

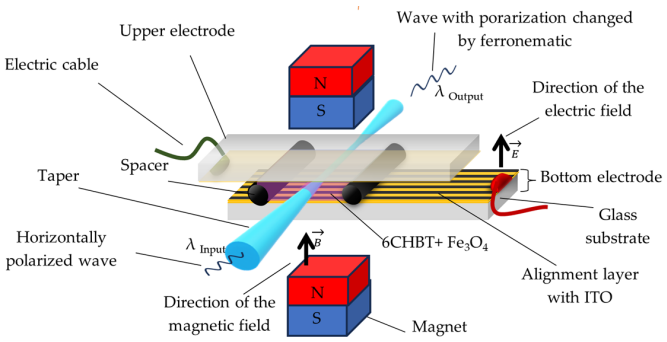

Fig. 1. Polarization measurement setup: scheme of the LC cell filled 6CHBT + Fe_3O_4

2.2. Magnetic nanoparticles (MNPs)

The synthesis of Fe_3O_4 MNPs was as in our previous report. In short, the procedure involved dissolving 1.5 g of $FeCl_2 \cdot 4H_2O$ and 5 g of $FeCl_3 \cdot 6H_2O$ in 100 ml of de-ionized ultrapure water. This mixture was heated to 90°C under vigorous stirring and an argon flow. Once heated, 0.8 ml of oleic acid and 10 ml of 25% NH_4OH aqueous solution were added, causing an immediate color change from orange to black, indicating the formation of magnetite (Fe_3O_4). The reaction continued for 15 minutes under the same conditions. After cooling, the magnetic precipitate was thoroughly rinsed with alternating deionized water and ethanol and then dried. The resulting Fe_3O_4 nanoparticles were examined. Powder X-ray diffraction (PXRD) confirmed the presence of magnetite (Malvern PANalytical Empyrean). Scanning transmission electron microscopy (STEM) reveals nanoparticles with an average diameter of around 10 nm (FEI Nova NanoSEM 450), which agrees well with dynamic light scattering (DLS) measurements (Malvern ZetaSizer NanoZS). The zeta potential of the nanoparticles in toluene is measured at approximately 0 mV. The detailed characteristics of the MNPs used in this research can be found in our previous report [39].

3. RESULTS AND DISCUSSION

The investigation was divided into two sections. The first section focused on measuring transmission parameters over a broad wavelength range of 1400–1600 nm. The selection of this spectral range was related to the single-mode operation of the optical fiber used. The lowest insertion loss was achieved within this range during the fabrication of the optical fiber tapers. Figure 2 presents the spectral characteristics for LC cells with various weight concentrations of MNPs: 0.0 wt% (pure 6CHBT), 0.1 wt%, 0.2 wt%, and 0.5 wt%. In each graph, the transmission measurement of an empty cell without LC filling was used as a reference. For this research, the steering voltage range was kept consistent across all LC cell types, from 0 to 160 V, without modulating the output signal. Measurements were conducted both with and without a magnetic field. The LC cells were fabricated with a perpendicular orientation of the alignment layer relative to the axis of the tapered optical fiber and were tested under identical external conditions. The cell filled with pure LC exhibited the highest transmission among all tested samples, with a maximum power value fluctuating around –42 dBm. However, it showed the lowest dynamic range change – approximately 1 dBm between the power level obtained at U = 160 V and the threshold power level at U = 20 V. In contrast, for LC cells filled with ferronematic mixtures, the power level strongly depended on the wavelength and was significantly lower than that of the pure LC. This reduction resulted from the introduction of MNPs, which caused increased attenuation.

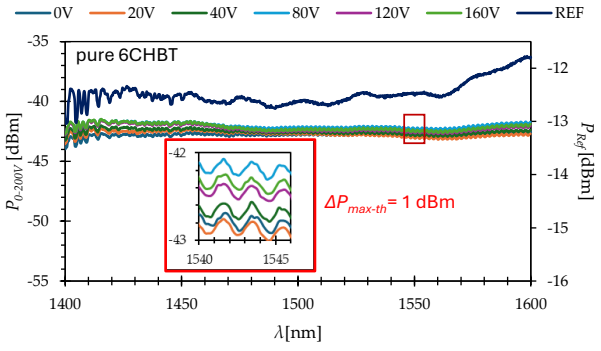

(a)

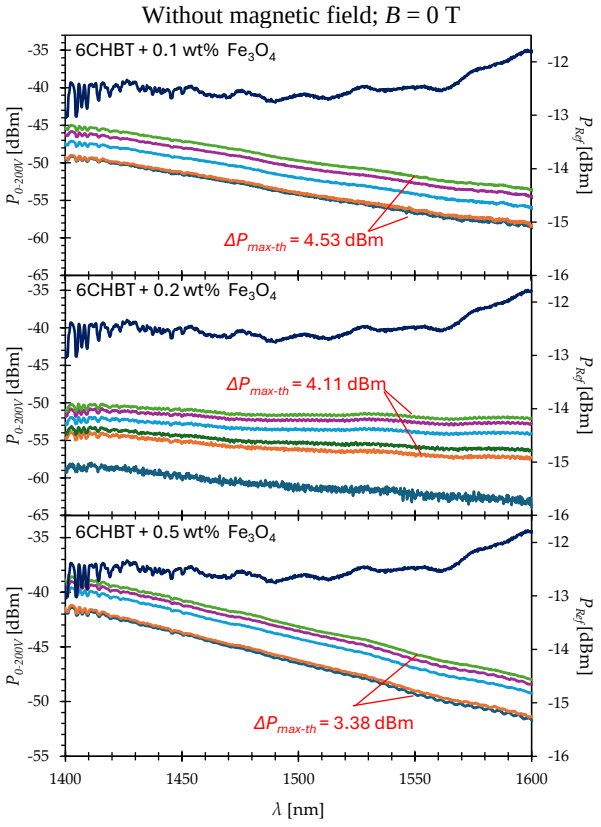

(b)

Fig. 2

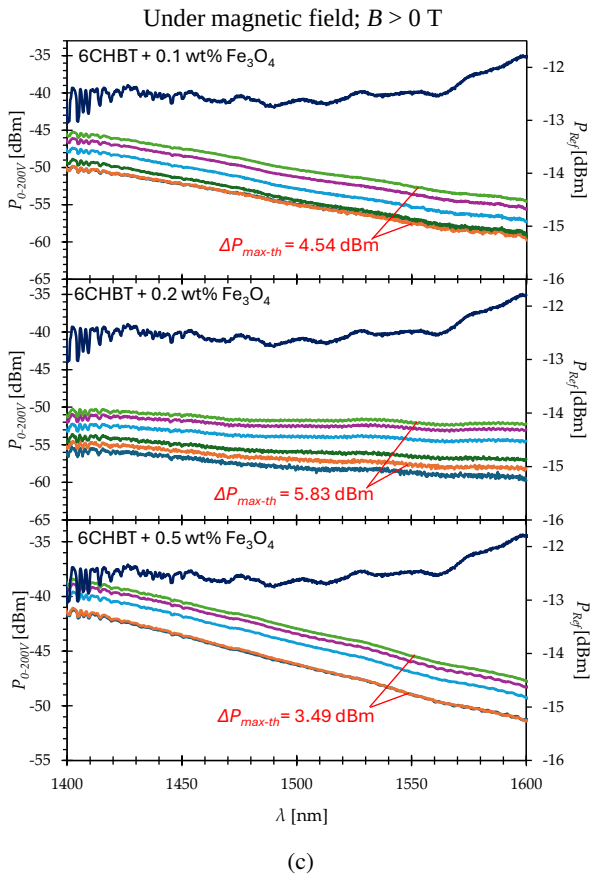

(c)

Fig. 2. Transmission spectra were obtained for the LC cell filled with (a) pure LC without a magnetic field and (b) ferronematic with different wt. concentration of Fe_3O_4 – 0.1 wt%; 0.2 wt%; 0.5 wt% without magnetic field; and (c) ferronematic with different wt. concentration of Fe_3O_4 – 0.1%; 0.2%; 0.5% with magnetic field

Furthermore, the transmission was influenced by the presence of a magnetic field. Accordingly, the graphs show the calculated values of the difference between the maximum and threshold power levels. In all cases, the dynamic range increased when both electric and magnetic fields were applied, with the highest difference observed for the 0.2 wt% concentration.

The second part of the measurement focused on polarization analysis. Measurements were conducted using a single-mode laser with a wavelength of 1550 nm, corresponding to single-mode propagation in SMF. The measurements were performed for both pure LC and LC mixed with magnetic nanoparticles. The main parameters measured were power, azimuth, and ellipticity, both with and without the presence of a magnetic field. In all cases, the initial polarization state was set to horizontal linear polarization using a mechanical polarization controller.

Figure 3 presents the results for LC cells filled with pure 6CHBT and those doped with 0.1 wt% Fe_3O_4. In this case, polarization measurements were conducted at various steering voltages UU, ranging from 20 to 160 V, with amplitude modulation (AM) at 1 Hz and 100% modulation depth. The 100% AM with a square waveform enables two distinct states: ON (corresponding to 100% of the applied voltage) and OFF (voltage turned off). Therefore, the power level was normalized for all LC cells to emphasize changes in the power dynamic range between the ON and OFF states. Liquid crystals are birefringent materials. As expected, an input plane wave with initial horizontal polarization changed to an elliptical one. In the case of pure LC, both the azimuth and ellipticity were negative, in-

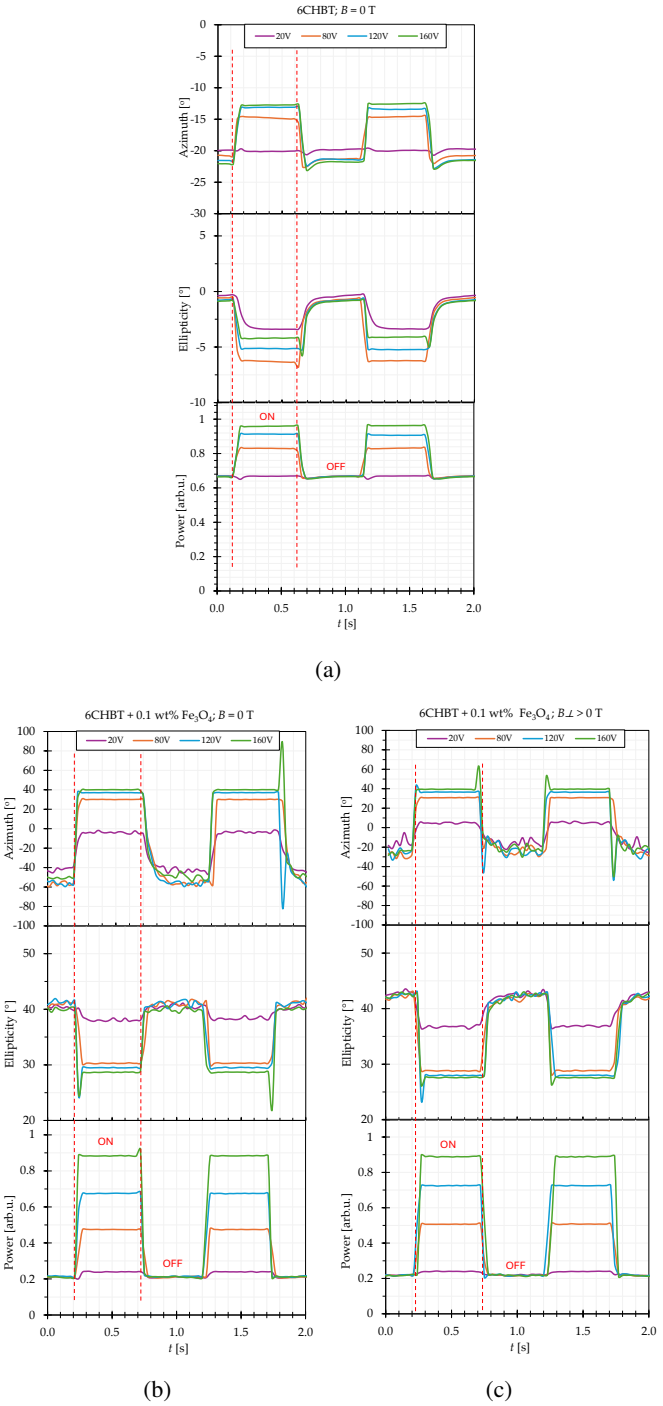

(a)

(b)

(c)

Fig. 3. The azimuth and ellipticity values, corresponding to the applied steering voltages ranging from 20 to 160 V, were obtained for LC cells filled with: (a) pure 6CHBT without a magnetic field, (b) 6CHBT with 0.1 wt% Fe_3O_4 without applied magnetic field; (c) LC doped with 0.1 wt% Fe_3O_4 with applied magnetic field

dicating left-handed elliptical polarization, with total changes of 10° and 6°, respectively. The applied electric field decreased the azimuth angle and increased the ellipticity.

Doping the liquid crystal with MNPs caused a significant change in the azimuth angle. In the case of the LC cell without a magnetic field, the maximum difference between the ON and OFF states reached nearly 100°, with the azimuth angle shifting from a negative to a positive value. Moreover, the ellipticity remained positive in this configuration, ranging from 40° to 30°, and decreased as the applied voltage increased. When the magnetic field was applied, the azimuth angle in the OFF state decreased to approximately −30°, while the maximum value in the ON state remained unchanged at 40°. Simultaneously, the magnetic field had minimal influence on the ellipticity.

The next tested MNP concentration in the LC was 0.2 wt%. The corresponding results, obtained with and without the application of a magnetic field, are presented in Fig. 4. Increasing the MNP concentration resulted in a substantial reduction in the azimuth angle. As in the previous case, the azimuth angle changed from a negative to a positive value, ranging from −15° to 10° without the magnetic field, and from −17° to 2° when the magnetic field was applied.

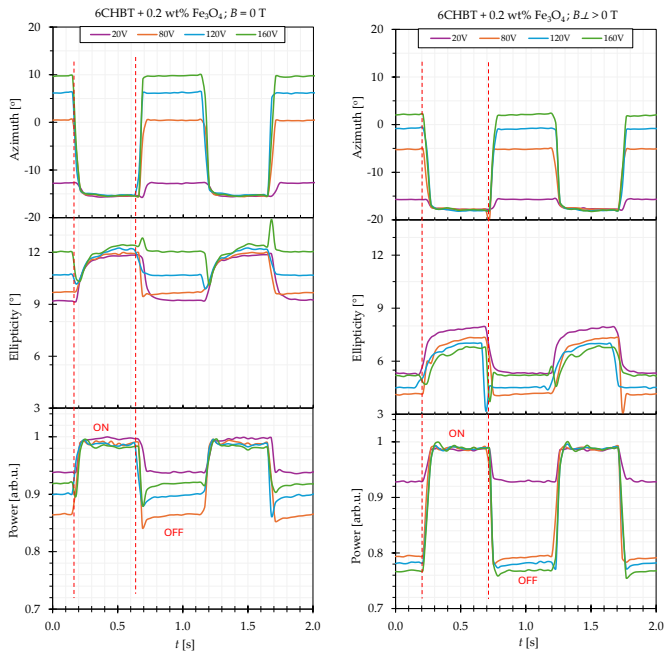

Fig. 4. The azimuth and ellipticity values, corresponding to the applied steering voltages ranging from 20 to 160 V, were obtained for LC cells filled with 6CHBT + 0.2 wt% Fe_3O_4: (a) without a magnetic field; (b) with the applied magnetic field

Additionally, the ellipticity of the LC with 0.2 wt% MNPs decreased. It remained positive but dropped to 12° without the magnetic field and to 7.5° with the magnetic field. The amplitude of ellipticity variation between the ON and OFF states in both cases (with and without the magnetic field) was small but nearly identical, at approximately 3.5°.

The final examined concentration was 0.5 wt% MNPs (Fig. 5). In this case, the azimuth angle remained negative and decreased as the steering voltage increased. The magnetic field had minimal influence on the azimuth, which varied between −7° and −13° in both measurement conditions. The ellipticity was very small, ranging from −2° to 2° without the magnetic field, and from −3° to 1° with the magnetic field.

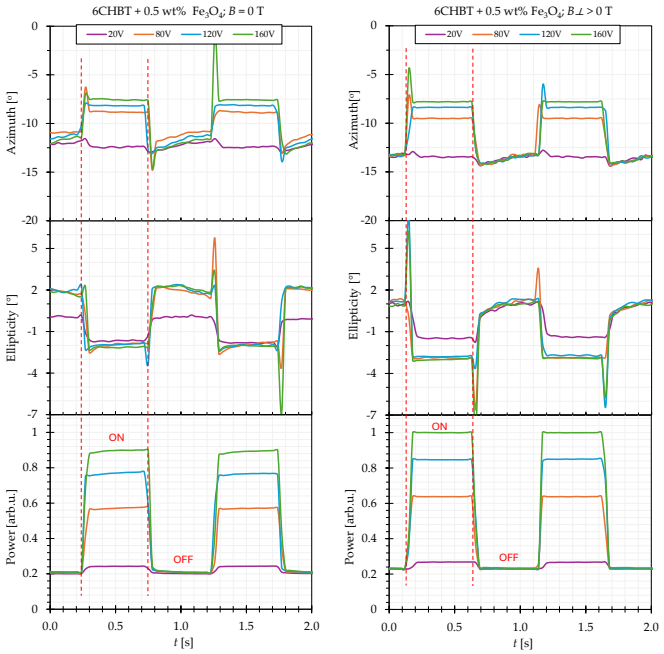

Fig. 5. The azimuth and ellipticity values, corresponding to the applied steering voltages ranging from 20 to 160 V, were obtained for LC cells filled with 6CHBT + 0.5 wt% Fe_3O_4 (a) without a magnetic field; (b) with the applied magnetic field

Unlike the other LC cells, above the steering voltage threshold of 20 V, the ellipticity remained nearly constant and was independent of the applied voltage.

The graphs obtained for both pure and doped liquid crystals demonstrate that the shape of the signal, in terms of azimuth and ellipticity, did not perfectly replicate the square-modulated input signal. The visible rounding of the response during ON/OFF switching is attributed to the extended response time of the LC cells. As demonstrated in our previous study [39], the response times are strongly dependent on the concentration of MNPs in the LC host. The rise and fall times, as calculated in [39], were found to be the shortest for 0.1 wt% Fe_3O_4 compared to all other concentrations and pure LC when subjected to an external electric field. Furthermore, it was observed that the influence of the magnetic field on the switching dynamics increases significantly with the MNP concentration. In the present study, a near-square response for all measured parameters was observed only in the case of the 0.1 wt% doped cell, confirming its superior switching speed. As shown, doping LCs with MNPs significantly affects polarization-related properties, particularly azimuth and ellipticity. To quantitatively evaluate the impact of

weight concentration and the presence of a magnetic field, the maximum changes in each parameter – Δ Azimuth, Δ Ellipticity, and Δ Power – under the influence of electric and magnetic fields were calculated. Below is an example calculation for Δ Azimuth at 0.1 wt% Fe_3O_4 without a magnetic field

$$\Delta_{\text{Azimuth}}(20\,V) = \text{Azimuth}_{\text{Max}}(20\,V) - \text{Azimuth}_{\text{Min}}(20\,V) = -5^\circ - (-47^\circ) = 42^\circ.$$

These calculations were also repeated for Δ Ellipticity and Δ Power for each LC cell, both with and without the magnetic field. The obtained results are presented in Fig. 6.

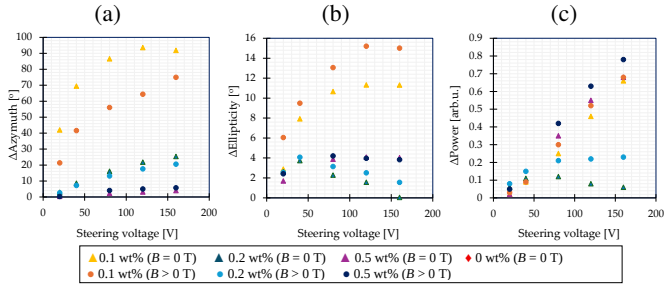

Fig. 6. Switching range of (a) azimuth, (b) ellipticity, and (c) power under electric and magnetic fields as a function of the wt% concentration of MNPs

Compared to pure LC (0.0 wt%), a significant change in Δ Azimuth was observed for the 0.1 wt% sample. A slight increase in this parameter was also noted for 0.2 wt%. In both cases, Δ Azimuth was higher without the magnetic field. For 0.5 wt%, the change in azimuth at a given steering voltage was the smallest, with Δ Azimuth falling below the value recorded for the pure LC. Regarding ellipticity, the 0.1 wt% MNP-doped LC exhibited the highest changes between different steering voltages. In contrast, Δ Ellipticity for the other concentrations was lower than that of pure 6CHBT. Additionally, Δ Ellipticity was consistently higher when a magnetic field was applied.

In terms of power, the highest changes (Δ Power) were observed for both 0.1 wt% and 0.5 wt% concentrations. In all tested cases, the presence of a magnetic field led to an increase in Δ Power.

In summary, the obtained polarization results indicate that a concentration of 0.1 wt% Fe_3O_4 significantly enhances key optical parameters, including azimuth and ellipticity, which is beneficial for sensing applications. However, it should be noted that increasing the concentration of MNPs results in higher optical losses due to light absorption by the nanoparticles and scattering effects. Moreover, LC molecules tend to anchor onto the nanoparticle surfaces, and at higher concentrations, this interaction can hinder the reorientation of LC molecules by disrupting the local order parameter. As a result, the switching effect becomes less pronounced.

The discrepancies observed between lower concentrations and the 0.5 wt% sample may also be attributed to the increased tendency of MNPs to spontaneously aggregate at higher concentrations. Agglomerated nanoparticles can settle at the bottom of the LC cell, reducing the effective concentration of active particles, and thus weakening the overall LC response – potentially bringing it close to that of the undoped material [45].

Additionally, it is important to note that this experiment used standard SMF, which is not a polarization-maintaining optical fiber. Therefore, future studies should explore the use of polarization-maintaining fibers to ensure greater stability and control of polarization-dependent effects.

4. CONCLUSIONS

The conducted research on the influence of doping LCs with varying weight concentrations of MNPs led to the following conclusions:

Dependence of polarization parameters on MNP concentration

The degree of doping significantly affects the behavior of azimuth and ellipticity. For the 0.1 wt% concentration, an exponential change in both parameters was observed, followed by stabilization above 120 V. In contrast, at higher doping levels, only small linear changes in azimuth were recorded, while the ellipticity remained relatively constant.

1. Pure 6CHBT exhibits left-handed elliptical polarization. Doping the LC with MNPs causes a shift in the polarization direction. At lower concentrations (0.1 wt% and 0.2 wt%), the polarization shifts to right-handed. At 0.5 wt%, only a narrow voltage-dependent switching range between left- and right-handed polarization was observed.
2. The application of a magnetic field enhances the differences in azimuth and ellipticity between the ON and OFF states. Specifically, the azimuth variation occurs over a narrower range, while the ellipticity increases. The most pronounced changes in both parameters were observed at the 0.1 wt% concentration. For the 0.2 wt% and 0.5 wt% concentrations, the changes were less significant or diminished.
3. This study demonstrates that doping LCs with 0.1 wt% Fe_3O_4 provides optimal performance in terms of polarization response and signal modulation. At higher concentrations, spontaneous agglomeration of MNPs likely occurred, resulting in a decline in performance due to reduced homogeneity and increased scattering or sedimentation.

The results also indicate that the performance of the proposed device can be further enhanced by using polarization-maintaining optical fibers. Despite this, the developed LC-based optical element already exhibits significant application potential – as a tunable wavelength filter or a multifunctional sensor for detecting temperature, magnetic fields, and/or electric fields.

Funding: This research was funded by the Program of the Republic of Poland – Research Grant MUT project no UGB 531-000031-W900-22.

REFERENCES

[1] R. Zhang *et al.*, "Advanced liquid crystal-based switchable optical devices for light protection applications: principles and strategies," *Light-Sci. Appl.*, vol. 12, p. 11, 2023, doi: 10.1038/s41377-022-01032-y.

[2] Y. Choi *et al.*, "Stimuli-Responsive Materials from Liquid Crystals," *ACS Appl. Opt. Mater.*, vol. 1, pp. 1879–1897, 2023, doi: 10.1021/acsaom.3c00282.

[3] M. Tsuei, M. Shivrayan, Y.K. Kim, S. Thayumanavan, and N.L. Abbott, "Optical 'Blinking' Triggered by Collisions of Single Supramolecular Assemblies of Amphiphilic Molecules with Interfaces of Liquid Crystals," *J. Am. Chem. Soc.*, vol. 142, pp. 6139–6148, 2020, doi: 10.1021/jacs.9b13360.

[4] J. Guardià, J.A. Reina, M. Giamberini, and X. Montané, "An Up-to-Date Overview of Liquid Crystals and Liquid Crystal Polymers for Different Applications: A Review," *Polymers*, vol. 16, p. 2293, 2024, doi: 10.3390/polym16162293.

[5] D. Devadiga, A. Tantri Nagaraja, D. Devadiga, and M. Selvakumar, "Minireview and Perspectives of Liquid Crystals in Perovskite Solar Cells," *Energy Fuels*, vol. 38, pp. 854–868, 2024, doi: 10.1021/acs.energyfuels.3c04050.

[6] V.P. Chavda *et al.*, "Lyotropic Liquid Crystalline Phases: Drug Delivery and Biomedical Applications," *Int. J. Pharm.*, vol. 647, p. 123546, 2023, doi: 10.1016/j.ijpharm.2023.123546.

[7] M. Chountoulesi, S. Pispas, I.K. Tseti, and C. Demetzos, "Lyotropic Liquid Crystalline Nanostructures as Drug Delivery Systems and Vaccine Platforms," *Pharmaceuticals*, vol. 15, p. 429, 2022, doi: 10.3390/ph15040429.

[8] M. Zatloukalova, L. Poltorak, R. Bilewicz, and J. Vacek, "Lipid-Based Liquid Crystalline Materials in Electrochemical Sensing and Nanocarrier Technology," *Microchim. Acta*, vol. 190, p. 187, 2023, doi: 10.1007/s00604-023-05727-w.

[9] A. d'Alessandro and R. Asquini, "Light Propagation in Confined Nematic Liquid Crystals and Device Applications," *Appl. Sci.*, vol. 11, p. 8713, 2021, doi: 10.3390/app11188713.

[10] J.E. Moś, K.A. Stasiewicz, and L.R. Jaroszewicz, "Investigation of transmission properties of a tapered optical fibre with gold nanoparticles liquid crystal composite cladding," *Opto-Electron. Review*, vol. 30, no. 4, 2022, doi: 10.24425/opelre.2022.143936.

[11] J. Jadżyn, L. Hellemans, G. Czechowski, C. Legrand, and Douai, "Dielectric and viscous properties of 6CHBT in the isotropic and nematic phases," *Liq. Cryst.*, vol. 1, pp. 613–619, 2010, doi: 10.1080/026782900202453.

[12] A. Sengupta, *Liquid Crystal Theory. Topological Microfluidics: Nematic Liquid Crystals and Nematic Colloids in Microfluidic Environment*, Switzerland: Springer, 2013, pp. 7–34, doi: 10.1080/15421406.2011.572784.

[13] V. Lacková *et al.*, "The collective ordering of magnetic nanoparticles in a nematic liquid crystal," *J. Magn. Magn. Mater.*, vol. 589, p. 171616, 2024, doi: 10.1016/j.jmmm.2023.171616.

[14] F. Baldini, A. Giannetti, A.A. Mencaglia, and C. Trono, "Fiber Optic Sensors for Biomedical Applications," *Curr. Anal. Chem.*, vol. 4, pp. 378–390, 2008, doi: 10.2174/157341108785914880.

[15] S. Zhang, Y. Peng, X. Wei, and Y. Zhao, "High-Sensitivity Biconical Optical Fiber SPR Salinity Sensor with a Compact Size by Fiber Grinding Technique," *Measurement*, vol. 204, p. 112156, 2022, doi: 10.1016/j.measurement.2022.112156.

[16] L. Huang *et al.*, "Fiber-Based Energy Conversion Devices for Human-Body Energy Harvesting," *Adv. Mater.*, vol. 32, p. 1902034, 2020, doi: 10.1002/adma.201902034.

[17] Y. Yao, M. Yan, and Y. Bao, "Measurement of cable forces for automated monitoring of engineering structures using fiber optic sensors: A review," *Autom. Constr.*, vol. 126, p. 103687, 2021, doi: 10.1016/j.autcon.2021.103687.

[18] A.T. Kurzych, L.R. Jaroszewicz, and J.K. Kowalski, "Development of Three-Axis Fibre-Optic Seismograph," *Sensors*, vol. 22, no. 22, 2022, doi: 10.3390/s22228902.

[19] B.A. Taha *et al.*, "Comprehensive Review Tapered Optical Fiber Configurations for Sensing Application," *Biosensors*, vol. 11, p. 253, 2021, doi: 10.3390/bios11080253.

[20] L. Chen *et al.*, "Ultrahigh-Sensitivity Label-Free Optical Fiber Biosensor," *Sens. Actuator B-Chem.*, vol. 320, p. 128283, 2020, doi: 10.1016/j.snb.2020.128283.

[21] B. Lee, "Review of the present status of optical fiber sensors," *Opt. Fiber Technol.*, vol. 9, pp. 57–79, 2003, doi: 10.1016/S1068-5200(02)00527-8.

[22] R.C. Jorgenson and S.S. Yee, "Control of the dynamic range and sensitivity of a surface plasmon resonance based fiber optic sensor," *Sens. Actuator. A-Phys.*, vol. 43, pp. 44–48, 1994, doi: 10.1016/0924-4247(93)00661-M.

[23] T.T. Larsen and A. Bjarklev, "Optical devices based on liquid crystal photonic bandgap fibres," *Opt. Express*, vol. 11, pp. 2589–2596, 2003, doi: 10.1364/OE.11.002589.

[24] S.-M. Kuo, Y.-W. Huang, S.-M. Yeh, W.-H. Cheng, and C.-H. Lin, "Liquid crystal modified photonic crystal fiber for electrical flux measurement," *Opt. Express*, vol. 19, pp. 18372–18379, 2011, doi: 10.1364/OE.19.018372.

[25] T.R. Woliński *et al.*, "Recent advances in liquid-crystal fiber-optics and photonics," *Proc. SPIE*, vol. 10125, 2017, doi: 10.1117/12.2261115.

[26] J. Tang *et al.*, "Optical fiber bio-sensor for phospholipase using liquid crystal," *Biosens. Bioelectron.*, vol. 170, p. 112547, 2020, doi: 10.1016/j.bios.2020.112547.

[27] J. Korec, K.A. Stasiewicz, L.R. Jaroszewicz, and K. Garbat, "SPR Effect Controlled by an Electric Field," *Materials*, vol. 13, no. 21, p. 4942, 2020, doi: 10.3390/ma13214942.

[28] P. Marc, K. Stasiewicz, J. Korec, L.R. Jaroszewicz, and P. Kula, "Polarisation properties of nematic liquid crystal cell," *Opto-Electron. Rev.*, vol. 27, no. 4, pp. 321–328, 2019, doi: 10.1016/j.opelre.2019.10.001.

[29] J.E. Lee, N. Lee, T. Kim, J. Kim, and T. Hyeon, "Mesoporous Silica Nanocomposite Nanoparticles," *Accounts Chem. Res.*, vol. 44, no. 10, pp. 893–902, 2011, doi: 10.1021/ar2000259.

[30] H. Barrak *et al.*, "Functionalisation of ZnO nanoparticles," *Arabian J. Chem.*, vol. 12, no. 8, pp. 4340–4347, 2019, doi: 10.1016/j.arabjc.2016.04.019.

[31] U. Hafeez, I. Khan, Z.H. Yamani, and A. Qurashi, "Synthesis of SnO2 nanoparticles," *Ultrason. Sonochem.*, vol. 34, pp. 484–490, 2017, doi: 10.1016/j.ultsonch.2016.06.025.

[32] K.A. Stasiewicz *et al.*, "In-Line Gas Sensor with a Graphene Oxide Layer," *Electronics*, vol. 12, p. 830, 2023, doi: 10.3390/electronics12040830.

[33] P.V.R.K. Ramacharyulu *et al.*, "Iron phthalocyanine modified mesoporous titania," *Phys. Chem. Chem. Phys.*, vol. 17, pp. 26456–26462, 2015, doi: 10.1039/C5CP03576G.

[34] I. Khan, K. Saeed, and I. Khan, "Nanoparticles: Properties, applications and toxicities," *Arab. J. Chem.*, vol. 12, no. 7, pp. 908–931, 2019, doi: 10.1016/j.arabjc.2017.05.011.

[35] K.A. Stasiewicz *et al.*, "Tapered Optical Fiber with Alkanes and Fe3O4," *Sensors*, vol. 22, p. 7801, 2022, doi: 10.3390/s22207801.

[36] P. Das *et al.*, "Co3O4 Nanoparticles-Coated Optical Fibers," *ACS Appl. Nano Mater.*, vol. 5, no. 7, pp. 8973–8981, 2022, doi: 10.1021/acsanm.2c01172.

[37] Y. Chen *et al.*, "Magnetic Nanoparticles Functionalized Few-Mode-Fiber," *Nanomaterials*, vol. 9, no. 5, p. 78, 2019, doi: 10.3390/nano9050785.

[38] Y. Zheng *et al.*, "Optical fiber magnetic field sensor," *Opt. Commun.*, vol. 336, pp. 5–8, 2015, doi: 10.1016/j.optcom.2014.09.026.

[39] M. Niewczas *et al.*, "Liquid crystal cladding with Fe3O4 nanoparticles," *Advanced Optical Technologies*, vol. 13, p. 1422695, 2024, doi: 10.3389/aot.2024.1422695.

[40] Corning Inc., "Product Information Sheet – PI-1424-AEN," [Online]. Available: https://www.corning.com/media/worldwide/coc/documents/Fiber/product-information-sheets/PI-1424-AEN.pdf [Accessed: Oct. 9, 2024].

[41] O. Frazao, J.L. Santos, F.M. Araujo, and L.A. Ferreira, "Optical sensing with photonic crystal fibers," *Laser Photon. Rev.*, vol. 2, pp. 449–459, 2008, doi: 10.1002/lpor.200810034.

[42] G. Brambilla, "Optical fibre nanowires and microwires: review," *J. Opt.*, vol. 12, p. 043001, 2010, doi: 10.1088/20408978/12/4/043001.

[43] S. Wang, S. Feng, S. Wu, Q. Wang, and L. Zhang, "Temperature sensor using graphene coated microfiber," *IEEE Photon. J.*, vol. 10, p. 6802008, 2018, doi: 10.1109/JPHOT.2018.2827073.

[44] J.W. Baran *et al.*, "Physical properties of mesogenic isothiocyanatobenzenes," *Mol. Cryst. Liquid Cryst.*, vol. 123, pp. 237–245, 1985, doi: 10.1080/00268948508074781.

[45] M. Hähsler, I. Appel, and S. Behrens, "Magnetic hybrid materials in liquid crystals," *Phys. Sci. Rev.*, vol. 7, no. 9, pp. 1009–1032, 2022, doi: 10.1515/psr-2019-0090.